



## Tunable polarization-induced Fano resonances in stacked wire-grid metasurfaces

Xavier Romain <sup>1,2</sup>✉, Riccardo Degl'Innocenti <sup>2</sup>, Fadi I. Baida<sup>1</sup> & Philippe Boyer<sup>1</sup>

Stacked metasurfaces are being investigated in light of exploring exotic optical effects that cannot be achieved with single-layered metasurfaces. In this article, we theoretically demonstrate that metallic wire-grid metasurfaces with specific polarization properties have the ability to induce tunable Fano resonances when they are stacked. The developed original model—combining a circulating field approach together with an extended Jones formalism—reveals the underlying principle that gives rise to the polarization-induced Fano resonances. The theoretical frame is validated in an experimental proof of concept using commercially available wire-grids and a terahertz time domain spectrometer. This unexplored possibility opens an alternative path to the realization and control of Fano resonances by using stacked metallic metasurfaces. Furthermore, these findings suggest that the polarization can be used as an additional degree of freedom for the design of optical resonators with enhanced and tunable properties.

<sup>1</sup>Département Optique - Institut FEMTO-ST UMR 6174, Université Bourgogne Franche-Comté - CNRS, Besançon, France. <sup>2</sup>Department of Engineering, Lancaster University, Bailrigg, Lancaster, UK. ✉email: [x.romain@lancaster.ac.uk](mailto:x.romain@lancaster.ac.uk)

Fano resonances<sup>1,2</sup> currently draw much attention because of their remarkable and unique potential for applications such as sensing with high quality factor<sup>3</sup>. Over the past decades, Fano resonances have been reported in a large variety of experimental configurations ranging from electromagnetic structures<sup>4–7</sup> to elastic structures<sup>8</sup>. Similar observations of Fano signature in electromagnetic metamaterials<sup>9</sup> were made by deliberately breaking the symmetry of the metamaterial unit-cell. These results have been rapidly followed by extensive studies on the coupling of trapped modes in metamaterials in order to obtain Fano resonances<sup>10</sup>. More recently, a vast literature focused on the excitation of tunable and/or multiple Fano lineshapes for increased functionalities<sup>11–14</sup>. At the same time, metallic metamaterials rose in popularity because of the wide diversity of physical effects which they can exhibit such as extraordinary optical transmission<sup>15</sup>, negative refraction<sup>16</sup> or perfect absorption<sup>17</sup>. However, the performances associated to these physical effects may be limited by the intrinsic physical properties of the unit-cell, or might require complex designs and fabrications. Stacked metasurfaces are currently proposed as an alternative way to achieve complex functionalities<sup>18</sup>. Besides, the interaction between metasurfaces brings further degree of freedom and enables additional effects<sup>19, 20</sup>. For example, stacked structures are currently proposed to efficiently manipulate the polarization of light<sup>21–24</sup>.

In this article, we demonstrate that metallic metasurfaces possessing basic polarization dependencies offer the possibility to induce Fano resonances when these metasurfaces are stacked. The main focus of the present work is not to report another polarization-dependent metasurface design where the unit cell itself is exciting Fano resonances<sup>25, 26</sup>, but rather to demonstrate, theoretically and experimentally, another route for the realization of Fano resonances via stacked metasurfaces. This concept is theoretically introduced and further developed thanks to an original cavity model which combines a circulating field approach<sup>27</sup> and an extended Jones formalism<sup>28</sup>. The theoretical study is experimentally supported by demonstrating tunable polarization-induced Fano resonances in the THz regime by using a THz time domain spectrometer and implementing Metallic Wire-Grid Metasurfaces (MWGMs). This unusual configuration to excite Fano resonances paves the way toward unconventional designs of tunable and high quality factor devices, which are in great demand in the THz region.

**Results and discussion**

**Theoretical background and principle.** The importance of the MWGMs linear polarization properties for exciting Fano resonances is first examined. An electromagnetic plane wave is considered to be propagating along the *z*-axis and falls in normal incidence on a stack of two parallel and perfectly conducting MWGMs, as shown in Fig. 1a, acting as linear polarizers. The transmission and reflection of the first MWGM, identifying the *x* and *y* axes, respectively, serve as a reference. The period, the thickness and the aperture width of both MWGMs are denoted by *p*, *h*, and *a* respectively. The distance between the two MWGMs is *d* and  $\theta$  is the rotation angle of the second MWGM with respect to the *x*-axis. The geometrical notations of the structure are summarized in Fig. 1a.

The stack of two MWGMs is assumed to form a Fabry-Perot-like (FP-like) cavity. To accurately describe the resonance and polarization properties of the FP-like cavity, a circulating field approach<sup>27</sup> is associated to a Jones formalism<sup>28</sup>, as illustrated in Fig. 1b. A scalar model (excluding polarization properties), reporting more details on the circulating field was thoroughly investigated in<sup>27</sup>. The steady state forward circulating field,  $\vec{E}_c$ , is

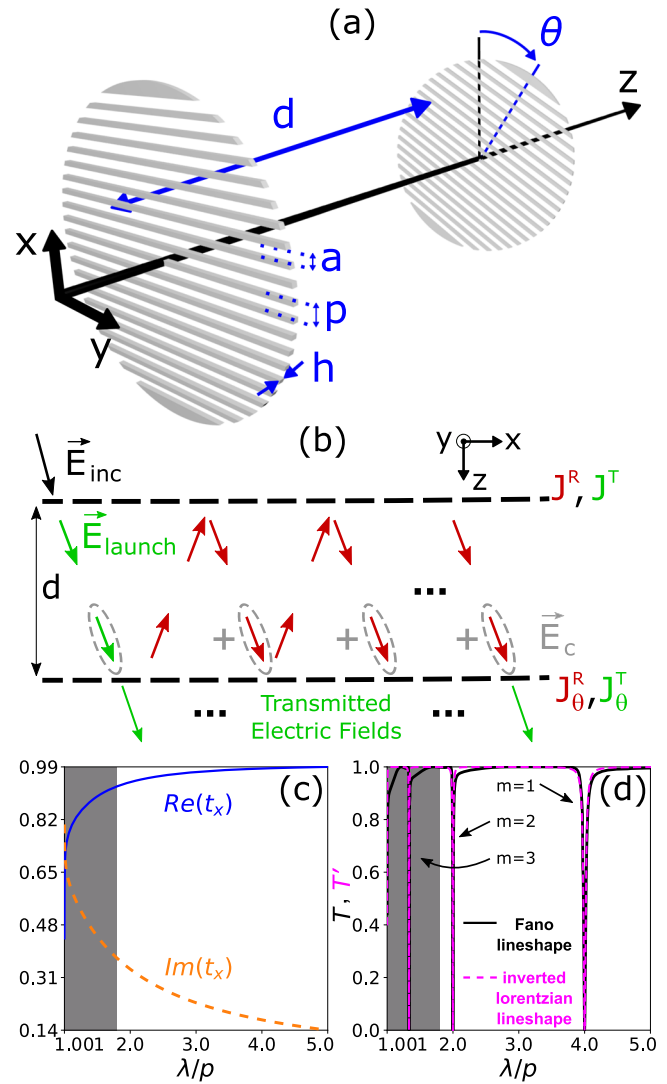


**Fig. 1 Structure description and principle.** **a** 3D illustration of two Metallic Wire-Grid Metasurfaces (MWGMs) stacked along the *z*-axis, separated by a distance *d*, where the second MWGM is rotated by an angle  $\theta$ . The thickness, the aperture width and the period are denoted by *h*, *a*, and *p*, respectively. **b** Principle of the Fabry-Perot-like (FP-like) cavity formed by two MWGMs characterized by their Jones matrices  $J^T, J^R$  and  $J^T_\theta, J^R_\theta$  respectively.  $\vec{E}_{\text{launch}}$  is the initial electric field entering the cavity, and  $\vec{E}_c$  is the steady state forward circulating field in the FP-like cavity. The arrows are deliberately tilted to clearly represent the round trips in the FP-like cavity. **c** Simulated spectra of  $t_x$ , the transmission coefficient along the *x*-axis for one MWGM where  $\lambda/p$  is the normalized wavelength. The real and imaginary parts of  $t_x$  are depicted in solid blue line and dashed orange line respectively, and computed with  $a/p = 0.9$  and  $h/p = 0.1$ . The grayed area specifies the spectral region ( $\lambda/p \leq 1.8$ ) for which the model has lower accuracy. **d** Simulated transmission spectra of the FP-like cavity with  $\theta = 10^\circ$  and  $d/p = 2.0$ . The integer *m* denotes the FP harmonic order where the Fano resonances occurs. The black curve shows the spectrum of the transmission *T* computed with the numerical values extracted from the monomode modal method. The dashed pink curve gives the spectrum of the transmission *T'* computed with the special case where  $t_x = 1$ .

given by

$$\vec{E}_c = J_c U \vec{E}_{\text{launch}} \tag{1}$$

where  $\vec{E}_c$  corresponds to the infinite sum of waves incoming on the second MWGM, as highlighted by the dashed gray ellipses in

Fig. 1b.  $J_c$  is the Jones matrix that accounts for the infinite round-trips in the cavity and its expression is detailed later in Eqs. (4)–(6). The propagation operator  $U = uI$  links the electric fields from the first to the second MWGM inside the FP-like cavity. The term  $I$  is a  $(2 \times 2)$  identity matrix,  $u = e^{id2\pi/\lambda}$  represents the phase shift accumulated by the electric field in half a round-trip and  $\lambda$  denotes the wavelength. The electric field  $\vec{E}_{\text{launch}}$ , is the initial field launched in the cavity and its expression is

$$\vec{E}_{\text{launch}} = J^T \vec{E}_{\text{inc}} \quad (2)$$

where

$$J^T = \begin{pmatrix} t_x & 0 \\ 0 & t_y \end{pmatrix} \text{ and } J^R = \begin{pmatrix} r_x & 0 \\ 0 & r_y \end{pmatrix} \quad (3)$$

are the transmission and reflection Jones matrices of the first MWGM where  $J^R$  is mentioned for completeness. The terms  $t_x$ ,  $t_y$  and  $r_x$ ,  $r_y$  are respectively the transmission and reflection coefficients along the  $x$  and  $y$  axes for one MWGM. The polarization-induced effect can be inferred from the expression of  $J_c$ , which is written as

$$J_c = [I - U^2 J^R J_\theta^R]^{-1} \quad (4)$$

where  $J_\theta^R = R(\theta) J^R R(-\theta)$  is the reflection Jones matrix of the second MWGM and  $R(\theta)$  is the rotation matrix.

The matrix  $J_c$  can be reformulated as

$$J_c = \begin{pmatrix} J_c^{xx} & J_c^{xy} \\ J_c^{yx} & J_c^{yy} \end{pmatrix} \quad (5)$$

which can be expanded into

$$J_c = \frac{1}{D} \begin{pmatrix} 1 - u^2 r_y (s^2 r_x + c^2 r_y) & u^2 c s (r_x - r_y) r_x \\ u^2 c s (r_x - r_y) r_y & 1 - u^2 r_x (c^2 r_x + s^2 r_y) \end{pmatrix} \quad (6)$$

where  $D = \det(I - U^2 J^R J_\theta^R)$ ,  $c = \cos\theta$  and  $s = \sin\theta$ . For this complex general case given by Eq. (6), it is fundamental to remark that the coupling terms  $J_c^{yx}$  and  $J_c^{xy}$  are vanishing if  $r_x = r_y$  - as it would be the case with polarization insensitive mirrors. In other words, the polarization properties of the MWGMs brings additional polarization coupling effects - inducing Fano resonances - that are not achievable in classical FP cavities. Other works using matrix formalism have analyzed anisotropic FP resonators<sup>29, 30</sup> or chiral FP interferometers<sup>31, 32</sup>. None of these studies, however, considered mirrors with polarization dependency, they rather employed classical FP cavities filled with anisotropic or optically active media. The linear polarization dependency of the MWGMs ( $r_x \neq r_y$ ) is the key difference that permits the excitation of Fano resonances.

**Theoretical and numerical investigations.** The transmission of the optical arrangement of Fig. 1a is numerically simulated with  $a/p = 0.9$ ,  $h/p = 0.1$ ,  $d/p = 2.0$  and  $\theta = 10^\circ$ . The transmission properties of one MWGM are first investigated. The spectral range of interest is  $\lambda/p \geq 2$  which ensures that only the fundamental transverse electromagnetic guided mode is excited in the MWGMs. Note that the fundamental guided mode is polarized along the periodicity axis, i.e., the  $x$ -axis. Using a monomodal method<sup>28</sup>, the coefficients  $t_x$  and  $r_x$  are numerically calculated by Airy-like expressions. The perfectly conducting metal hypothesis imposes that the two other coefficients  $t_y$  and  $r_y$  are 0 and  $-1$ , respectively. This further implies that the electric field  $\vec{E}_{\text{launch}}$  is polarized along the  $x$ -axis. Figure 1c represents the spectra of the real and imaginary parts of  $t_x$  in solid blue line

and dashed orange line, respectively. The transmission  $T$  of the FP-like cavity is defined as

$$T = |J_{\text{FP}}^{T,xx}|^2 + |J_{\text{FP}}^{T,yx}|^2 \quad (7)$$

with

$$J_{\text{FP}}^T = J_\theta^T J_c U J^T \quad (8)$$

where  $J_{\text{FP}}^T$  is the transmission Jones matrix of the FP-like cavity and  $J_\theta^T = R(\theta) J^T R(-\theta)$  is the transmission Jones matrix of the second MWGM. Note that the transmission results achieved by this formalism are strictly identical to the transmission values computed by the S-matrix propagation algorithm<sup>33</sup>. Figure 1d yields the transmission spectrum of the cavity in solid black line computed for  $d/p = 2.0$  and  $\theta = 10^\circ$ . Clear Fano-like resonances appear at the FP resonance condition expressed as

$$\lambda = \frac{2d}{m} \quad (9)$$

where  $m$  denotes the FP harmonic order with  $m \in \mathbb{N}$ . It is worth emphasizing that the Fano dip asymmetry increases as  $\lambda$  decreases. However, the grayed area for which  $\lambda/p \leq 1.8$  is the region where higher order modes are guided in the MWGMs and the monomodal modal method reaches a lower computation accuracy for  $t_x$ .

To further explain the origin of these Fano resonances, the lower FP harmonic  $m = 1$  is analyzed in more details. At  $\lambda/p = 4.0$ , the coefficients are  $t_x = 0.985 + 0.169i$  and  $r_x = 0.475 \times 10^{-2} + 0.028i$ . For explanatory purposes, it is now assumed that  $t_x = 1$  and  $r_x = 0$ . In this ideal and almost realistic scenario the matrix  $J_c$  reduces to

$$J_c = \begin{pmatrix} 1 & 0 \\ -\frac{u^2 c s}{1 - u^2 c^2} & \frac{1}{1 - u^2 c^2} \end{pmatrix}. \quad (10)$$

This specific peculiar case is interesting from a theoretical perspective as it helps elucidating the physical mechanism which gives rise to Fano resonances. To highlight the core principle responsible for the polarization-induced Fano resonance, it is now essential to distinguish three cases:

- (1) When the MWGMs are aligned ( $\theta = 0^\circ$ ), the coupling terms are  $J_c^{xx} = J_c^{yy} = 0$ . This configuration yields  $J_c^{yy} = 1/(1 - u^2)$  corresponding to the electric field Airy distribution of a perfect y-polarized FP resonance referred to as  $\text{FP}_y$ . At the same time, Eq. (8) becomes

$$J_{\text{FP}}^T = J^T J_c U J^T = \begin{pmatrix} u & 0 \\ 0 & 0 \end{pmatrix} \quad (11)$$

which represents an x-polarized single pass propagation operator. The x-polarized field  $\vec{E}_{\text{launch}}$  does not couple to the  $\text{FP}_y$  resonance and simply propagates through the structure. Therefore, the  $\text{FP}_y$  resonance is not excited or, in other words, it is “trapped” in the FP-like cavity.

- (2) When the MWGMs are crossed ( $\theta = 90^\circ$ ), the coupling terms are  $J_c^{xx} = J_c^{yy} = 0$  which prevents again the coupling of the  $\text{FP}_y$  dark mode. In addition, the transmission vanishes as it is expected for two crossed polarizers.
- (3) When the MWGMs are not aligned, nor crossed ( $\theta \neq 0^\circ$  and  $\theta \neq 90^\circ$ ), the coupling of  $\vec{E}_{\text{launch}}$  to the  $\text{FP}_y$  resonance occurs via the term  $J_c^{xx}$ . As it is numerically demonstrated in Fig. 1d, such coupling induces a Fano resonance according to the FP resonance condition given by Eq. (9). The single pass x-polarized electric field and the “trapped”  $\text{FP}_y$  resonance might be regarded as an analog of bright and dark modes respectively, that are exploited to excite Fano resonances<sup>10</sup>.

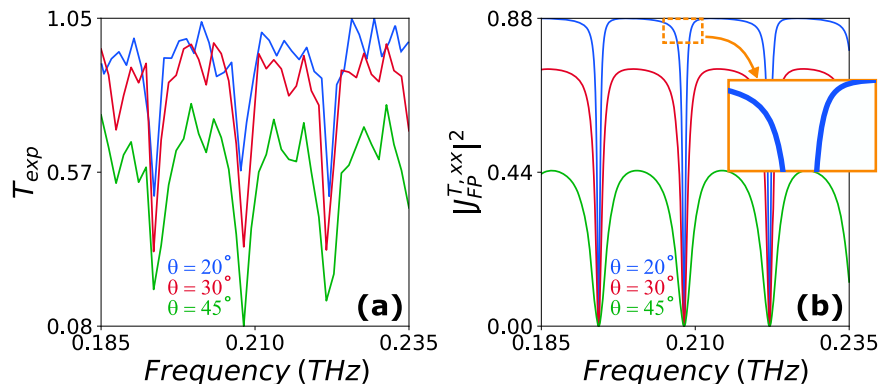


**Fig. 2 Experimental and theoretical comparison.** **a** Measured and **b** computed transmission spectra for  $p = 35 \mu\text{m}$ ,  $a = 25 \mu\text{m}$ ,  $h = 10 \mu\text{m}$  and  $d = 1, 08 \text{ cm}$  where  $p$ ,  $a$  and  $h$  are the MWGM's period, aperture width and thickness, respectively, and  $d$  is the distance between them. The inset in **(b)** highlights the slight asymmetry in the Fano line shape.

Finally, for this special case where  $t_x = 1$  and  $r_x = 0$ , the transmission  $T'$  through the FP-like cavity is

$$T' = \left| \frac{u(1 - u^2)}{1 - u^2 \cos^2 \theta} \right|^2 \cos^2 \theta \quad (12)$$

which is consistent with the transmission expression reported in ref. <sup>33</sup>. The FP resonance condition, as stated by Eq. (9), corresponds to the case where  $u = 1$  and therefore leads to  $T' = 0$ ,  $\forall \theta \neq 0 \pmod{\pi}$ . The expression of  $T'$  at the FP resonance condition produces inverted Lorentzian line shapes, as depicted by the dashed pink curve in Fig. 1d. The results presented in Fig. 1d are also compatible with Eq. (17) of ref. <sup>6</sup> which predicts symmetric line shapes “when either  $r$  or  $t$  is zero”. As shown in Fig. 1c, when  $\lambda \rightarrow \infty$ , the coefficient  $t_x \rightarrow 1$  ( $r_x \rightarrow 0$ ) which causes the Fano line shape to be less asymmetric. This is clearly observed in Fig. 1d where the transmission  $T$  gets closer to the symmetric inverted Lorentzian transmission  $T'$  as  $\lambda \rightarrow \infty$ .

It is important to note that, in Eq. (10), the coupling term  $J_c^{yx}$  can be controlled by  $\theta$ . It further suggests that the spectral width of the polarization-induced Fano resonances can be tuned by acting on  $\theta$ , as previously observed in ref. <sup>33</sup>. From Eq. (12) we derive an expression of the quality factor  $Q$  for the inverted Lorentzian line shape which is given by

$$Q = \frac{m\pi}{2\sin^{-1}(\frac{1}{2}\sin\theta \tan\theta)} \quad (13)$$

where  $\theta$  is expressed in radian. This expression further confirms that the polarization-induced Fano resonance can be spectrally tailored by controlling  $\theta$ . It also suggests that  $Q$  theoretically tends to infinity when  $\theta \rightarrow 0$ .

**Experimental demonstration.** The polarization-induced Fano resonance and its spectral tunability are demonstrated in a proof-of-principle experimental configuration in the THz region (see Methods section). Note that the THz range is particularly relevant and suited to verify the developed theoretical model as metals are close to be considered as perfect electric conductors at these frequencies. Figure 2a represents the normalized transmission spectra experimentally acquired for the different angles  $\theta$  and Fig. 2b depicts the computed counterpart using the FP-like cavity model. The measured and simulated results reported in Fig. 2a, b, respectively, exhibit a good agreement only limited by the available spectrometer resolution and by the signal to noise ratio. Note that for this considered spectral range  $t_x = 0.998 + 0.053i \approx 1$  which causes the Fano lineshape to be almost symmetric as highlighted in the inset of Fig. 2b. The quality factor of these

quasi-symmetric Fano line shapes can be assessed using Eq. (13). The resonance close to 0.210 THz corresponds to the FP order  $m = 15$  and  $Q = 386$ , 162 and 65 respectively for  $\theta = 20^\circ$ ,  $30^\circ$ , and  $45^\circ$ . The 1.2 GHz spectrometer resolution does not allow for  $\theta$  below  $20^\circ$  as the Fano line width would become narrow enough to be undetected by the spectrometer. For example, for  $\theta = 1^\circ$ , we theoretically obtain  $Q = 1.55 \times 10^5$  with an associated linewidth of 1.35 MHz. Such results - arising from the simplest possible proof of concept - are promising for the future designs of THz devices with high quality factors. Further investigations will focus on a stack of two metasurfaces sharing a THz compatible substrate such as Si/SiO<sub>2</sub>. The polarization-induced Fano resonances could be implemented in actively tunable optoelectronic THz platforms<sup>34</sup> where the mechanical tuning can be replaced and superseded by graphene-covered tunable metasurfaces<sup>35, 36</sup> with modulation speed beyond 100 MHz<sup>37</sup>.

## Conclusion

In conclusion, stacked MWGMs with linear polarization dependency have been theoretically investigated in order to explore an efficient and alternative strategy to induce and control Fano resonances. The experimental proof of principle was performed in the THz range showing very good agreement with the predicted trends. It is worth stressing the versatility and generalization of this alternative way to realize Fano resonances by using FP-like cavities. This different approach does not require metasurfaces that are specially designed with complex unit-cells or custom-made materials. Rather, the polarization-induced Fano resonance addresses fundamental concepts of optics as it essentially relies on simple polarization properties and basic resonance effects. This principle could therefore be extended to other metasurfaces made of unit-cells featuring the same linear polarization properties<sup>28</sup>. Likewise, the polarization-induced Fano resonance is not restricted to the THz domain and it could be scaled to any other frequency ranges such as the near infrared or the visible regime. However, the larger metal absorption and the fabrication requirements would raise new challenges. Nonetheless, the diverse range of materials' optical responses available at those frequencies, such as Kerr effect or Pockels effect, may unlock other possibilities. As another interesting direction, the polarization-induced mechanism could be combined to other effects available in stacked metasurfaces to enhance the performances of integrated THz devices or to unveil more exotic optical responses.

## Methods

A pair of commercially available MWGMs from PureWavePolarizer (<https://www.purewavepolarizers.com/wire-grid-polarizers/10-micron-wire-far-ir-thz-polarizer>) is placed in a simple polarizer-analyzer configuration, which is also depicted in Fig. 1a. The geometrical parameters are  $p = 35 \mu\text{m}$ ,  $a = 25 \mu\text{m}$ ,  $h = 10 \mu\text{m}$ , and  $d = 1, 08 \text{ cm}$ .

The two MWGMs are inserted into a Menlo Systems Tera K15 THz time domain spectrometer based on photoconductive antennas (<https://www.menlosystems.com/products/thz-time-domain-solutions/terak15-terahertz-spectrometer/>). The maximal spectral resolution of the spectrometer is 1.2 GHz in the range of 0.1 THz to 3.5 THz. The first MWGM's transmission axis is aligned to the polarization direction of the photoconductive emitter. A set of transmission measurements, denoted by  $T(\theta)$ , are acquired at different relative angles of the second MWGM, i.e., for  $\theta = 20^\circ, 30^\circ$ , and  $45^\circ$ . The transmission  $T_0$ , measured at  $\theta = 0^\circ$ , serves as a reference for the normalized transmission  $T_{\text{exp}}$  which is defined as

$$T_{\text{exp}} = \frac{T(\theta)}{T_0}. \quad (14)$$

In order to be commensurate with the detector's polarization sensitivity along the  $x$ -axis only, the transmission  $T_{\text{exp}}$  has to be compared with  $|J_{\text{FP}}^{\text{Tx}}|^2$ , the  $x$ -axis component of the transmission coefficient given by the FP-like cavity model.

## Data availability

The raw data used for the experimental demonstration reported in Fig. 2a are available at <https://doi.org/10.17635/lancaster/researchdata/463>. All other data are available from the corresponding author upon request.

Received: 14 July 2020; Accepted: 6 May 2021;

Published online: 03 June 2021

## References

- Fano, U. Effects of Configuration Interaction on Intensities and Phase Shifts. *Phys. Rev.* **124**, 1866 (1961).
- Limonov, M. F., Rybin, M. V., Poddubny, A. N. & Kivshar, Y. S. Fano resonances in photonics. *Nat. Phot.* **11**, 543 (2017).
- Singh, R. et al. Ultrasensitive terahertz sensing with high-Q Fano resonances in metasurfaces. *Appl. Phys. Lett.* **105**, 171101 (2014).
- Fan, S. Sharp asymmetric line shapes in side-coupled waveguide-cavity systems. *Appl. Phys. Lett.* **80**, 908 (2002).
- Fan, S. & Joannopoulos, J. D. Analysis of guided resonances in photonic crystal slabs. *Phys. Rev. B* **65**, 235112 (2002).
- Fan, S., Suh, W. & Joannopoulos, J. Temporal coupled-mode theory for the Fano resonance in optical resonators. *JOSA A* **20**, 569–572 (2003).
- Lee, H.-T. & Poon, A. W. Fano resonances in prism-coupled square micropillars. *Opt. Lett.* **29**, 5 (2004).
- Goffaux, C. et al. Evidence of Fano-like interference phenomena in locally resonant materials. *Phys. Rev. Lett.* **88**, 225502 (2002).
- Fedotov, V. A., Rose, M., Prosvirnin, S. L., Papasimakis, N. & Zheludev, N. I. Sharp trapped-mode resonances in planar metamaterials with a broken structural symmetry. *Phys. Rev. Lett.* **99**, 147401 (2007).
- Singh, R., Rockstuhl, C., Lederer, F. & Zhang, W. Coupling between a dark and a bright eigenmode in a terahertz metamaterial. *Phys. Rev. B* **79**, 085111 (2009).
- Koshelev, K., Lepeshov, S., Liu, M., Bogdanov, A. & Kivshar, Y. Asymmetric metasurfaces with high-Q resonances governed by bound states in the continuum. *Phys. Rev. Lett.* **121**, 193903 (2018).
- Yang, L. et al. Characteristics of multiple Fano resonances in waveguide-coupled surface plasmon resonance sensors based on waveguide theory. *Sci. Rep.* **8**, 2560 (2018).
- Fu, H. et al. Independently tunable ultrasharp double fano resonances in coupled plasmonic resonator system. *IEEE Phot. J.* **10**, 1 (2018).
- Zhou, C. et al. Tunable Fano resonator using multilayer graphene in the near-infrared region. *Appl. Phys. Lett.* **112**, 101904 (2018).
- Ebbesen, T. W., Lezec, H. J., Ghaemi, H. F., Thio, T. & Wolff, P. A. Extraordinary optical transmission through sub-wavelength hole arrays. *Nature* **391**, 667 (1998).
- Smith, D. R., Pendry, J. B. & Wiltshire, M. C. K. Metamaterials and negative refractive index. *Science* **305**, 788 (2004).
- Landy, N. I., Sajuyigbe, S., Mock, J. J., Smith, D. R. & Padilla, W. J. Perfect metamaterial absorber. *Phys. Rev. Lett.* **100**, 207402 (2008).
- Cheng, H., Liu, Z., Chen, S. & Tian, J. Emergent functionality and controllability in few-layer metasurfaces. *Adv. Mater.* **27**, 5410 (2015).
- Liu, N. et al. Three-dimensional photonic metamaterials at optical frequencies. *Nat. Mater.* **7**, 31 (2008).
- Chen, S., Zhang, Y., Li, Z., Cheng, H. & Tian, J. Empowered layer effects and prominent properties in few-layer metasurfaces. *Adv. Opt. Mater.* **7**, 1801477 (2019).
- Boutria, M., Oussaid, R., Van Labeke, D. & Baida, F. I. Tunable artificial chirality with extraordinary transmission metamaterials. *Phys. Rev. B* **86**, 155428 (2012).
- Pfeiffer, C., Zhang, C., Ray, V., Guo, L. J. & Grbic, A. High performance bianisotropic metasurfaces: asymmetric transmission of light. *Phys. Rev. Lett.* **113**, 023902 (2014).
- Fan, R.-H. et al. Freely tunable broadband polarization rotator for terahertz waves. *Adv. Mater.* **27**, 1201 (2015).
- Romain, X., Baida, F. I. & Boyer, P. Spectrally tunable linear polarization rotation using stacked metallic metamaterials. *J. Opt.* **19**, 085102 (2017).
- Wu, C. et al. Spectrally selective chiral silicon metasurfaces based on infrared Fano resonances. *Nat. Commun.* **5**, 3892 (2014).
- Liu, Z. et al. 3D conductive coupling for efficient generation of prominent Fano resonances in metamaterials. *Sci. Rep.* **6**, 27817 (2016).
- Ismail, N., Kores, C. C., Geskus, D. & Pollnau, M. Fabry-Perot resonator: spectral line shapes, generic and related Airy distributions, linewidths, finesses, and performance at low or frequency-dependent reflectivity. *Opt. Express* **24**, 16366 (2016).
- Boyer, P. Jones matrices of perfectly conducting metallic polarizers. *JOSA A* **31**, 1226 (2014).
- Doyle, W. M. & White, M. B. Properties of an anisotropic Fabry-Perot resonator. *JOSA* **55**, 1221 (1965).
- Mamaev, Y. A. & Khandokhin, P. A. Nonorthogonal polarisation eigenstates in anisotropic cavities. *Quantum Electr.* **41**, 571 (2011).
- Silverman, M. P. & Badoz, J. Interferometric enhancement of chiral asymmetries: ellipsometry with an optically active Fabry-Perot interferometer. *JOSA A* **11**, 1894 (1994).
- Timofeev, I. V. et al. Geometric phase and o-mode blueshift in a chiral anisotropic medium inside a Fabry-Pérot cavity. *Phys. Rev. E* **92**, 052504 (2015).
- Romain, X., Baida, F. & Boyer, P. Extended Malus law with terahertz metallic metamaterials for sensitive detection with giant tunable quality factor. *Phys. Rev. B* **94**, 045407 (2016).
- Kindness, S. J. et al. Active control of electromagnetically induced transparency in a Terahertz metamaterial array with graphene for continuous resonance frequency tuning. *Adv. Opt. Mater.* **6**, 1800570 (2018).
- Kindness, S. J. et al. Graphene-integrated metamaterial device for all-electrical polarization control of terahertz quantum cascade lasers. *ACS Photon.* **6**, 1547 (2019).
- Kindness, S. J. et al. A terahertz chiral metamaterial modulator. *Adv. Opt. Mater.* **8**, 2000581 (2020).
- Jessop, D. S. et al. Graphene based plasmonic terahertz amplitude modulator operating above 100 MHz. *Appl. Phys. Lett.* **108**, 171101 (2016).

## Acknowledgements

X.R. and R.D. acknowledges support from the EPSRC (Grant No. EP/S019383/1).

## Author contributions

X.R. developed the theoretical model, undertook the theoretical and numerical analysis and made the experimental demonstration. X.R. wrote the manuscript with the supervision of R.D., F.I.B., and P.B. All the authors contributed to the discussion of the manuscript.

## Competing interests

The authors declare no competing interests.


## Additional information

**Supplementary information** The online version contains supplementary material available at <https://doi.org/10.1038/s42005-021-00623-2>.

**Correspondence** and requests for materials should be addressed to X.R.

**Reprints and permission information** is available at <http://www.nature.com/reprints>

**Publisher's note** Springer Nature remains neutral with regard to jurisdictional claims in published maps and institutional affiliations.

 **Open Access** This article is licensed under a Creative Commons Attribution 4.0 International License, which permits use, sharing, adaptation, distribution and reproduction in any medium or format, as long as you give appropriate credit to the original author(s) and the source, provide a link to the Creative Commons license, and indicate if changes were made. The images or other third party material in this article are included in the article's Creative Commons license, unless indicated otherwise in a credit line to the material. If material is not included in the article's Creative Commons license and your intended use is not permitted by statutory regulation or exceeds the permitted use, you will need to obtain permission directly from the copyright holder. To view a copy of this license, visit <http://creativecommons.org/licenses/by/4.0/>.

© The Author(s) 2021